

# A Study by Means of Electron Microscopy and Electron Diffraction of the Phase Transformation and the Domain Structure in $\text{Ag}_2\text{Te}$

C. MANOLIKAS

*Department of Solid State Physics, University of Thessaloniki,  
Thessaloniki, Greece*

Received October 3, 1985; in revised form April 22, 1986

The domain structure, observed in the low-temperature phase of  $\text{Ag}_2\text{Te}$  by means of electron diffraction and conventional electron microscopy, is interpreted on the basis of the crystallographical relationship between the low- and high-temperature phases. Diffuse scattering effects associated with the  $\beta \rightarrow \alpha$  transformation are also discussed. © 1987 Academic Press, Inc.

## 1. Introduction

Silver chalcogenides have been the subject of detailed experimental studies for a long time because of the superionic properties they exhibit at relatively low temperatures. Among these compounds silver telluride has been studied the least. Most of the work on that compound has been devoted to its phase transformations and to the corresponding crystal structures, but as far as is known from the literature, very little work has been done on the domain structure of the low-temperature phase.

It is the aim of this work to determine the structural variants and the interfaces which constitute this domain structure. A brief survey of the literature data concerning the structure will initially be given.

## 2. Structural Aspects

Silver telluride appears in three modifications, encountered at room, intermediate, and high temperatures. Only the first two

phases will be discussed here, denoted as  $\beta$ - and  $\alpha$ - $\text{Ag}_2\text{Te}$ , respectively. The phase transition temperature, as determined by a variety of experiments, varies from 132 to 157°C (1-5).

The structure of  $\alpha$ - $\text{Ag}_2\text{Te}$ , as reported by Rahlfs (6), is fcc, with lattice spacing  $a = 6.572\text{\AA}$  at 250°C and the space group  $Fm\bar{3}m - O_h^5$ . The tellurium atoms are in a cubic close-packed arrangement with the silver atoms distributed in various proportions on the tetrahedral, octahedral, and triangular interstices.

With regard to  $\beta$ - $\text{Ag}_2\text{Te}$ , different investigators have reported that its lattice is monoclinic or orthorhombic. A review of the literature data concerning the reported unit cells of  $\beta$ - $\text{Ag}_2\text{Te}$  is given in Table I with the following remarks:

1. The unit cell given by Tokody (7) is wrong, as already discussed by Frueh (10).

2. The orthorhombic cell given by Rowland and Berry (9) was derived from a crystal growth above the transition temperature and does not therefore correspond to the low-temperature form.

TABLE I  
CRYSTALLOGRAPHICAL DATA OF  $\beta$ -Ag<sub>2</sub>Te ACCORDING TO THE LITERATURE

Unit cell	Lattice parameters (Å)	Space group	Ref.
Monoclinic	$a = 6.57, b = 6.14, c = 6.10, \beta = 61^\circ 15'$	$Pm, P2, P2/m$	(7)
Orthorhombic	$a = 13.0, b = 12.7, c = 12.2$	—	(8)
Orthorhombic	$a = 16.28, b = 26.68, c = 7.55$	$Immm$	(9)
Monoclinic	$a = 8.09, b = 4.48, c = 8.96, \beta = 123^\circ 20'$	$P2_1/c$	(10, 11)
Monoclinic	$a = 8.15, b = 4.47, c = 8.09, \beta = 112^\circ 40'$	$P2_1/n$	(12)

3. The unit cell given by Terao and Berghezan (12) ( $a', b', c'$ ) can be transformed to the cell of Frueh ( $a, b, c$ ) by the relation:  $\bar{a}' = -(\bar{a} + \bar{c})$ ,  $\bar{b}' = b$ ,  $\bar{c}' = \bar{a}$ .

A complete analysis of the structure of  $\beta$ -Ag<sub>2</sub>Te has been carried out by Frueh (10). The model suggested by him is shown in Fig. 1. As he has noted, tellurium as well as silver atoms in this model are very close to their appropriate crystallographic positions in the fcc structure.

### 3. Specimen Preparation

Silver telluride was synthesized by heating a stoichiometric mixture of the constituents in an evacuated, sealed silica tube at 700°C. Single crystals were grown by melting the material, following by slow cooling to room temperature.

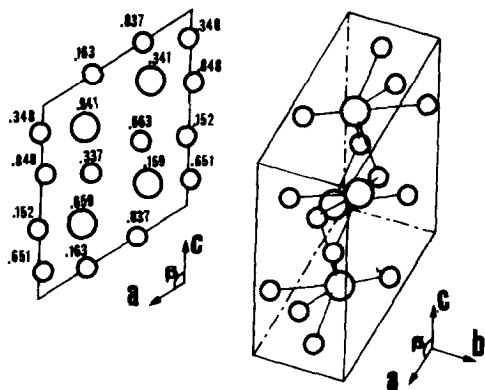


FIG. 1. Structural model for  $\beta$ -Ag<sub>2</sub>Te after Frueh (10).

Specimens suitable for electron microscopic observations were prepared by slicing the crystal, forming disks of 3-mm diameter, mechanical thinning, and final thinning by ion bombardment.

## 4. Observations and Results

### 4.1 $\alpha$ -Ag<sub>2</sub>Te

The heating of the specimen was done *in situ* in a JEM-100CX electron microscope by using the heating goniometer specimen holder. The use of this specimen holder allowed us to locate the transition temperature at  $150 \pm 2^\circ\text{C}$ .

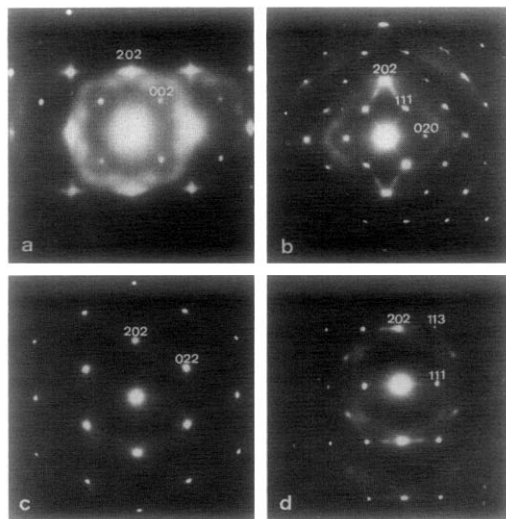


FIG. 2. Diffraction patterns along various sections of the reciprocal lattice of  $\alpha$ -Ag<sub>2</sub>Te: (a) 010, (b) 110, (c) 111, and (d) 211 section.

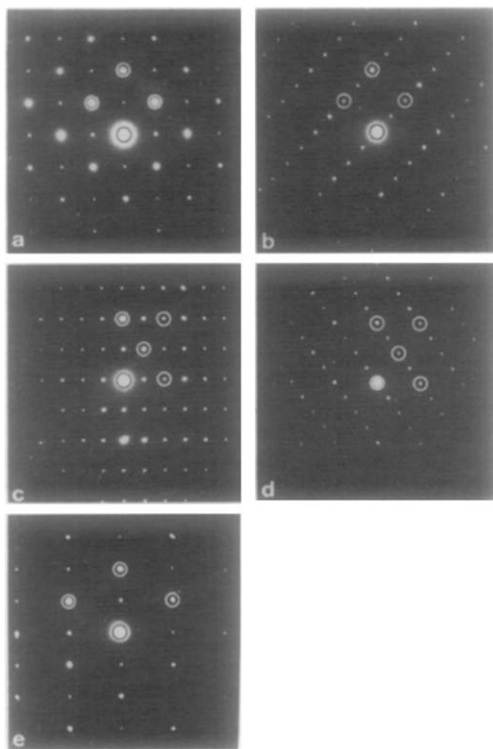


FIG. 3. Diffraction patterns corresponding to various sections of reciprocal lattice of  $\beta$ -Ag<sub>2</sub>Te. Circled spots show the fundamental fcc reflections: (a) and (b) correspond to the  $100_{fcc}$  section, (c) and (d) to the  $110_{fcc}$  section, and (e) to the  $111_{fcc}$  section.

The diffraction patterns from different sections of the high-temperature phase ( $\alpha$ -Ag<sub>2</sub>Te), some of which are reproduced in Fig. 2, disclose that this phase exhibits an average fcc structure with unit-cell parameter  $a \approx 6.6 \text{ \AA}$ .

Apart from the diffraction spots, strong diffuse scattering appears in these diffraction patterns, revealing disordering of silver atoms among the interstitial sites of tellurium sublattice. The diffuse scattering is concentrated mainly on curved surfaces close to the 200 cubic reflections. Nevertheless, weaker diffuse scattering exists between the spots along the four equivalent [111] cubic directions, with a maximum intensity midway between the fundamental spots.

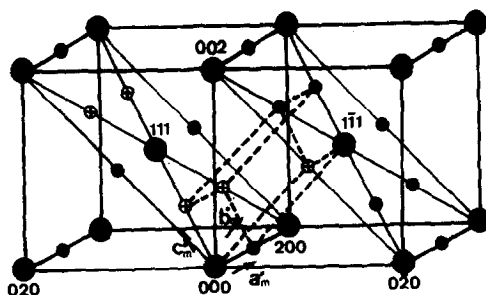


FIG. 4. Reciprocal lattice of  $\beta$ -Ag<sub>2</sub>Te. Large and small circles correspond to fundamental and superstructure reflections. Crossed circles show the forbidden superstructure reflections. The reciprocal unit cell corresponding to the Frueh's monoclinic unit cell is outlined by dashed lines.

#### 4.2 $\beta$ -Ag<sub>2</sub>Te

By cooling the specimen through the transition temperature the diffuse scattering vanishes and new reflections appear in the diffraction patterns. Repeated heating and cooling cycles through the transition point reveal that the same section of the reciprocal lattice of the  $\alpha$ -phase may produce different patterns of the reciprocal lattice of  $\beta$ -phase. Such sections of the  $\beta$ -phase are reproduced in Fig. 3.

On the basis of these diffraction patterns the reciprocal lattice of  $\beta$ -Ag<sub>2</sub>Te can be constructed (Fig. 4). It consists of the fundamental and superlattice and of forbidden reflections, represented by large, small, and crossed circles, respectively.

In the original reciprocal lattice the unit cell shown by dashed lines can be chosen. It corresponds to a primitive monoclinic real unit cell with constants  $a = 8.09 \text{ \AA}$ ,  $b = 4.48 \text{ \AA}$ ,  $c = 8.96 \text{ \AA}$ , and  $\beta = 123.4^\circ$ , i.e., it corresponds to the Frueh's unit cell (10). Indexing of the reciprocal lattice on the basis of this unit cell also leads to the  $P2_1/c$  space group.

The relationship between the monoclinic unit cell and the fundamental fcc one, as deduced from the common in the two reciprocal lattices reflections, is

$$\bar{a} = \frac{1}{2}(\bar{a}_1 - \bar{a}_2) + \bar{a}_3, \quad \bar{b} = \frac{1}{2}(\bar{a}_1 + \bar{a}_2), \\ \bar{c} = \bar{a}_2 - \bar{a}_1,$$

$\bar{a}_1 \bar{a}_2 \bar{a}_3$  being the fcc base vectors.

Assuming that, in first approximation, the Te atoms retain their positions in the two phases, the latter relationship between the two unit cells may be illustrated as in Fig. 5.

### 4.3 The Domain Structure of $\beta$ -Ag<sub>2</sub>Te

**4.3.1 Orientation variants.** Since in the  $\alpha \rightarrow \beta$  transition the symmetry of the structure is reduced from  $m\bar{3}m$  of order 48 for the  $\alpha$ -phase to  $2/m$  of order 4 for the  $\beta$ -phase, formation of  $48/4 = 12$  orientation variants is expected in the latter phase. They can be deduced from the elements of the variant generating group (V.G.G), which in the present case is  $23$  or  $\bar{3} 2/m$  (13).

Among these variants there exist "similar" ones, i.e., variants related by similarity operations of the V.G.G. They can be distinguished by further breaking the V.G.G. into simpler point groups, i.e.,

$$\{23\} = \{3\} \cdot \{m\} \cdot \{m'\}.$$

Each of these point subgroups produce "similar" orientation variants. The first one,  $\{3\} = \{E, C_1^3, C_2^3\}$ , yields the orientation variants having the monoclinic [201] direction parallel with each cubic edge (see Fig. 5); the second one,  $\{m\} = \{E, m\}$ , gives rise to those interchanging the directions of the monoclinic  $b$  and  $c$  axis, and the last one,  $\{m'\} = \{E, m'\}$ , to those differing in the orientation of the monoclinic  $\alpha$ -axis.

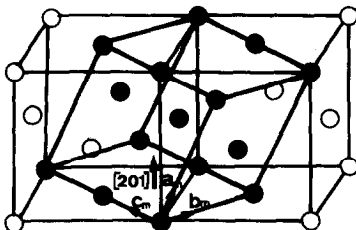


FIG. 5. Crystallographic relation between the unit cells of  $\alpha$ - and  $\beta$ -Ag<sub>2</sub>Te.

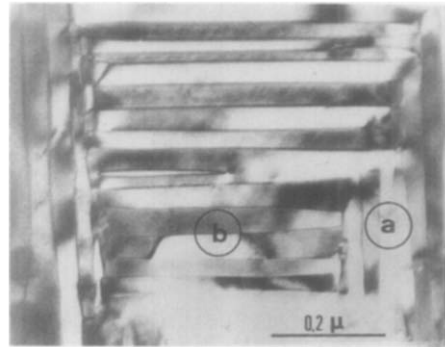


FIG. 6. Typical pattern of two  $\{3\}$ -type orientation variants. The monoclinic [201] directions are mutually perpendicular in adjacent domains and the boundaries between them coincide with the set of mutually perpendicular planes, bisecting the angles between the former directions.

Orientation variants of the  $\{3\}$  type are shown in Fig. 6. As deduced from the diffraction patterns taken across the boundaries between them (Fig. 7), the monoclinic [201] directions are mutually perpendicular in adjacent domains. Moreover, the boundaries coincide with the set of mutually perpendicular  $(110)_{\text{fcc}}$  planes which bisect the angle between the two [201] directions. They are actually the zero-strain interfacial planes between these variants.

Orientation variants of the  $\{m\}$  type cannot be distinguished from diffraction patterns as easily as the former ones. A combination of diffraction and contrast observations was applied in order to verify their occurrence. A typical pattern of such

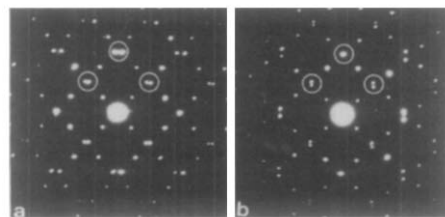


FIG. 7. Diffraction patterns taken across the boundaries between two  $\{3\}$ -type variants shown in Fig. 5. Note that the splitting of spots is perpendicular to the plane of the corresponding boundary.

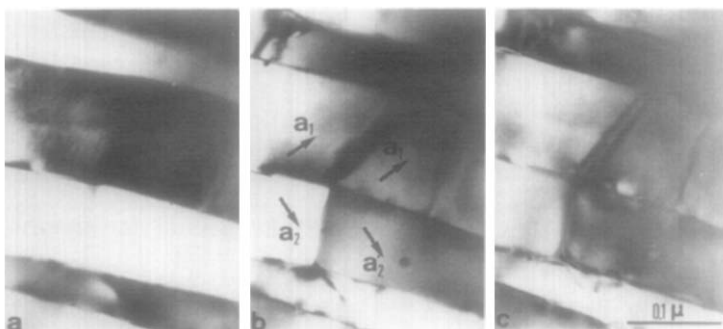


FIG. 8.  $\{m\}$ -type orientation variants in coexistence with  $\{3\}$ -type ones. The three patterns have been taken under different diffraction conditions. Arrows indicate the  $[201]$  directions in the different domains.

variants is shown in Fig. 8. The three images have been taken under different contrast conditions and disclose that each  $\{3\}$ -type variant may be further broken into two  $\{m\}$  type ones, the boundary between them generally being an arbitrary plane.

Because the reciprocal lattices for such variants completely coincide, a distinction by diffraction observations between the  $\{m'\}$ -type variants is not possible. Only differences in contrast arising from the differences in the structure factor of coinciding reflections would permit their distinction. Such orientation variants have intentionally been looked for, particularly in dark field images made in superlattice diffraction

spots; however, no evidence for their occurrence has been found.

**4.3.2 Translation variants.** Aside from the orientation, translation variants are also expected in the  $\beta$ -phase (Fig. 9). Since the ratio of the volumes of the primitive unit cells of the two phases is 4, there must also be four translation variants and, therefore, three different types of antiphase boundaries between them (13). The corresponding translation vectors are

$$\bar{R}_1 = \frac{1}{2}[201], \bar{R}_2 = \frac{1}{2}[001], \bar{R}_3 = \frac{1}{2}[111];$$

the indices refer to the monoclinic unit cell.

## 5. Discussion

In first approximation we can assume that the diffuse scattering in  $\alpha$ -Ag<sub>2</sub>Te is due to the static and dynamic disorder of the silver atoms within a rigid fcc lattice formed by tellurium atoms. The similar case of diffuse scattering in the bcc  $\alpha$ -Ag<sub>2</sub>Se has been discussed by de Ridder *et al.* (14) on the basis of the same assumption. They have further postulated that disorder causes small displacements of the silver atoms from their crystallographic positions which lead to the diffuse scattering. An alternate discussion of the diffuse scattering in the fast ion conductors can be done on the basis of the "liquid-like model" (15) using computational methods. This work is in pro-

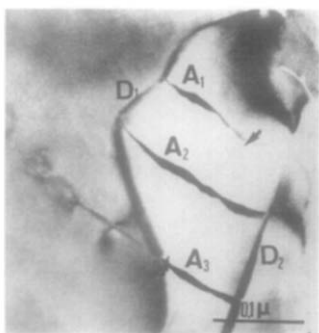


FIG. 9. Antiphase boundaries (A) in  $\beta$ -Ag<sub>2</sub>Te. Arrows indicate the trace of one more antiphase boundary which is almost in extinction. Boundaries between orientation variants (D) are also visible.

gress; the results will be published elsewhere.

Concerning the ordered  $\beta$ -Ag<sub>2</sub>Te, our electron diffraction data confirm the structure model suggested by Frueh (10). Furthermore, the crystallographic orientation relationship between the lattices in the two phases emerges from our results, so that one can easily determine the corresponding crystallographic positions of the silver atoms in the fcc lattice, as well as the displacements of the atoms from their ideal fcc positions.

The domain structure which  $\beta$ -Ag<sub>2</sub>Te exhibits as a result of ordering of the silver atoms consists theoretically of 12 orientation and 4 translation variants.

Apart from the orientation variants due to the different orientation of the monoclinic  $a$  axis, the other variants have been identified by our observations. The reason for the absence of variants differing in the orientation of the  $a$  axis is not clear. Presumably, they do not exist separately from the other orientation variants, and this makes their distinction difficult.

## References

1. V. V. CORBACHEV AND I. M. PUTLIN, *Inorg. Mater.* **11**, 1329 (1976).
2. N. G. DHERE AND A. GOSUAMI, *Thin Solid Films* **5**, 137 (1970).
3. S. A. ALIEV AND E. I. NIKULIN, *Inorg. Mater.* **13**, 607 (1977).
4. Y. IZUMI AND S. MIYATANI, *J. Phys. Soc. Japan* **35**, 312 (1973).
5. C. PAPANODITIS, *J. Phys. Radium* **23**, 411 (1962).
6. P. RAHLFS, *Z. Phys. Chem. Abt. B* **31**, 156 (1936).
7. L. TOKODY, *Z. Kristallogr.* **82**, 154 (1932); **89**, 416 (1934).
8. V. KOERN, *Naturwissenschaften* **27**, 432 (1939).
9. J. F. ROWLAND AND L. G. BERRY, *Amer. Mineral.* **36**, 471 (1939).
10. A. J. FRUEH, *Z. Kristallogr.* **112**, 44 (1959); *Amer. Mineral.* **46**, 645 (1961).
11. C. CHING-LIANG, R. M. IMAMOV, AND Z. G. PINSKER, *Kristallografiya* **6**, 772 (1961).
12. N. TERAQ AND A. BERGHEZAN, *C.R. Acad. Sci. Paris, Ser. B* **281**, 357 (1965).
13. G. VAN TENDELOO AND S. AMELINCKX, *Acta Crystallogr. Sect. A* **30**, 431 (1974).
14. R. DE RIDDER AND S. AMELINCKX, *Phys. Status Solidi A* **18**, 99 (1973); **23**, 615 (1974).
15. T. SAKUMA, K. IIDA, K. HONMA, AND H. OKASAKI, *J. Phys. Soc. Japan* **43**, 538 (1977).